77th IIW Annual Assembly and International Conference on Welding and Joining 7-12 July 2024 Rhodes, Greece

Effects of cooling rate on the microstructure and properties of coarse-grained zone in complex steel 780HE

Yue Wang[1], Xuetao Li[1], Shan Jiang[1], Xianchun Dong[1], Bing Yu[1]

[1]Research Institute of Technology of Shougang Group Co., Ltd., Beijing 100043, China

Abstract. A thermomechanical simulator Gleeble-3800 was used to simulate the thermal cycles experienced by coarse-grained zone of 780HE under different cooling rates during the welding process. The effects of cooling rates on the microstructure, precipitates, and mechanical properties of the coarse grain zones were systematically studied. Results showed that the cooling rates had no significant effect on the types of microstructure, which were all composed of lath bainite and granular bainite. When $t_{8/5}$ was 15s and 20s, the precipitates were almost only TiN. (Ti,Nb)C and (Ti,Nb,Mo)C reprecipitated when $t_{8/5}$ increased to 30s. As the cooling rate decreased, the yield strength and tensile strength first slightly decreased and then increased, while the uniform elongation changed opposite. The impact properties were significantly decreased as the cooling rates decreased.

1 Introduction

With the increasing attention to environmental protection and energy conservation, lightweighting had become an inevitable trend for the sustainable development of the automotive industry[1,2]. The chassis weight was approximately 30% of the total vehicle, and its lightweight design can effectively reduce fuel consumption. The torsion beam and control arm were important components of the chassis, and their lightweight prospect was promising. Various advanced high-strength steel with 800MPa grade had been developed for the fabrication of torsion beams and control arms[3,4]. For structural components, welding was an essential process, and the performance of welding joints directly affected there service life.

The welding performance of 800 MPa grade high-strength steel with thin gauge was the focus of researches. M. Zhang et al. [5] studied the weldability of Ti microalloyed steel CP800. No cold or low-temperature cracks were detected in the heat affected zones after welding, and the tensile strength of the joints were greater than 620 MPa. L. Yang et al.[6] investigated the effect of heat input on the microstructure and properties of 2.8mm CP800 laser welded joints. Results shew that under different heat inputs, the overall hardness of the welded joint was higher than that of CP800, while the elongation was opposite. Researches shew that the 800MPa grade complex steel had good weldability, and the mechanical properties of welded joints met the requirements for use. However, the temperature in the welding heat affected zone, especially the coarse-grained zone, increased sharply during welding, leading to severe grain coarsening and a decrease in the mechanical properties of the welded joint. At present, there was still a lack of research on improving the performance of coarse-grained zones.

In this paper, a thermomechanical simulator simulator Gleeble 3800 was used to conduct heat treatment at different cooling rates on 780HE with microalloyed elements Ti, Nb, and Mo added, to simulate the thermal cycling process experienced by coarse-grained zones during welding. The effects of the cooling rate on the microhardness, microstructure, precipitates, and mechanical properties of coarse-grained zones were systematically analyzed, which can provide theoretical support for studying and improving the welding properties of high-strength complex phase steel.

2 Materials and methods

The 4mm 800MPa grade high expansion steel 780HE with Ti, Nb, and Mo added was used in this study, and the specific chemical composition and mechanical properties are shown in Tables 1 and 2, respectively. The phase transformation curve of 780HE was measured using a DIL402C thermal dilatometer, ant the Ac1, Ac3 and Ar3 measured using the tangent method were 812 ℃ , 910 ℃ and 846℃, respectively.

Table 1. Chemical composition of 780HE (%)

C	Mo	Nb	Ti	N
0.05	0.16~0.20	0.035~0.045	0.08~0.12	0.004

Table 2. Mechanical properties of 780HE

Yield strength /MPa	Tensile strength /MPa	Uniform elongation /%	Impact energy /J
796	843	13.8	64.73

The thermomechanical simulator Gleeble 3800 was used to simulate the thermal cycles experienced by coarse-grained zone during the welding process. The samples were heated at 300 ℃/s to the peak temperature of 1320 ℃ and held for 0.5 s, the cooling curves were calculated based on the Rykalin-2D formula. The cooling times from 800 ℃ to 500 ℃ ($t_{8/5}$) were set as 15 s, 20 s, and 30 s to study the changes in hardness, microstructure, and mechanical properties at different cooling rates of the coarse-grained zone. In

the thermal simulation test, the temperatures of the samples were measured by a type-K thermocouple, which was welded to the center of the samples. Fig. 1 showed the schematic diagrams of thermal simulation samples used for tensile test and impact test. The samples used for impact tests had a V-shaped groove after thermal simulation, and the longitudinal axis of the samples were parallel to the rolling direction. The actual measured thermal cycle curves in thermal simulation process were shown in Fig. 2.

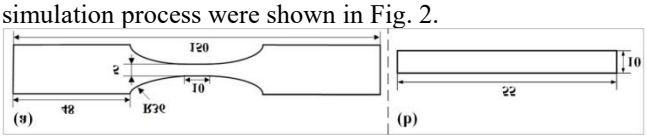

Fig. 1. Schematic diagram of thermal simulation samples: (a) tensile; (b) impact

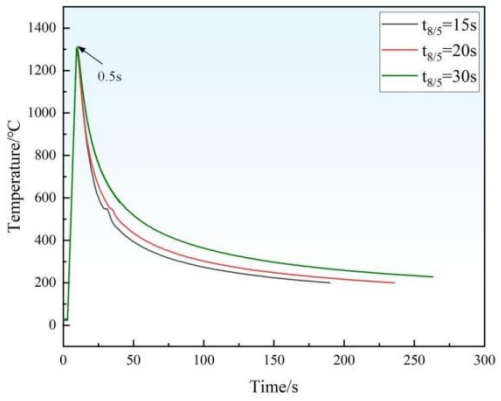

Fig. 2. The measured thermal cycle curves of the coarse-grained zone samples with different cooling rates

After thermal simulation, the middle parts of the samples were removed for mechanical grinding and polishing. 4vol% nital solution was used to etch the samples for microstructure observations via JSM-7001F scanning electron microscope (SEM), and the software Image Pro was used to calculate the relative content of each phase in the microstructure. The full width at half maximum (FWHM) and residual austenite in 780HE and coarse-grained samples were characterized by X-ray diffraction (XRD). For electron backscattered diffraction (EBSD) analysis, the samples were electrolytically polished at 15 V in a solution of 10vol% perchloric acid in alcohol. EBSD mappings were performed by TESCAN GAIA3 (accelerating voltage: 20kV, step size: 0.3μm for low magnification and 0.06μm for high magnification) to acquire the crystal structure information, and then analyzed by AZtecCrystal. The precipitates were extracted by carbon extraction replica, and characterized by transmission electron microscopy (TEM). The types of precipitates were determined by energy-dispersive X-ray spectroscopy (EDX). The average number of precipitates under 10 fields of view was used as the precipitation density. When calculating the initial precipitation temperatures of the precipitates, the element with a low mass fraction was used as the benchmark, and the other element was calculated using the ideal chemical ratio. The surface oxide skin of the samples was ground off before the tensile test and impact test, and the average value of three tests was taken as the results of yield strength, ultimate strength, total elongation, and impact energy.

3 Results

3.1 Microhardness

The microhardness values of 780FB and the coarse-grained samples with different cooling rates were shown in Table 3. Compared with 780HE, the coarse-grained zone softened, and as the cooling rate decreased, the softening phenomenon in the coarse-grained region weakened. When $t_{8/5}$ was 15s, the microhardness value was 258 HV. When $t_{8/5}$ increased to 20 s and 30 s, the microhardness values increased to 267 HV and 275 HV, respectively.

Table 3. The microhardness of 780HE and coarse grain zones with different cooling rates

$t_{8/5}$/s	780HE	15	20	30
Microhardness/HV	279	258	267	275

3.2 Microstructures

The microstructure of 780HE consisted of ferrite, bainite, and MA (martensite and austenite) islands, as shown in Fig. 3. The contents of ferrite bainite and were 54.5% and 37.6%, respectively, with the average grain size of 2.06 μm. The lath of bainite was about 344 nm, and the MA islands were distributed at the grain boundary, as shown in Fig. 4(b).

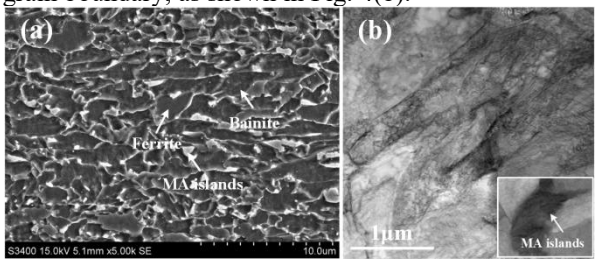

Fig. 3 780HE: (a) SEM and (b) TEM microstructures

Fig. 4 showed the microstructure of the coarse-grained zone with different cooling rates at the peak temperature of 1320 ℃. When $t_{8/5}$ was between 15s and 30s, the microstructure of coarse-grained zone was composed of lath bainite and granular bainite. Compared with 780HE, the grain sizes of the coarse-grained zones increased significantly. With the cooling rate decreased, the lath bainite content decreased, the width of bainite lath increased, and the average grain size increased. When $t_{8/5}$ was 15s, the lath bainite content was 91%, the granular bainite content was 9%, and the average grain size was 58.31 μm, as shown in Fig. 5 (a). The width of the bainite laths was about 620 nm (Fig. 5(b)). When $t_{8/5}$ was 20s, the lath bainite content was 88%, the width of the bainite laths was 656 nm, and the average grain size was 61.55nm, as shown in Fig. 5(c)(d). As $t_{8/5}$ increased to 30s, the lath bainite content decreased to 87%, the width of the bainite lath was 668 nm, and the average grain size was 66.67 nm, as shown in Fig. 5(e)(f).

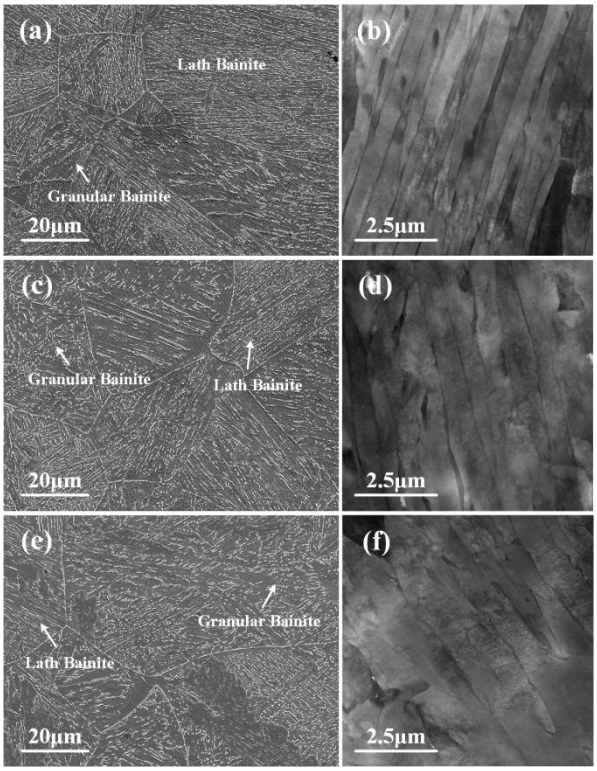

Fig. 4. SEM and TEM microstructures of coarse-grained zone samples with different cooling rates: (a) (b) 15 s; (c) (d) 20 s; (e) (f) 30 s.

3.3 Precipitates

The precipitate morphologies of 780HE and the coarse-grained samples with different cooling rates observed under TEM were shown in Fig. 5. According to the EDX analysis, the types of precipitates in each sample were similar, including square TiN, elliptical (Ti,Nb)C and circular (Ti,Nb,Mo)C. The average size of TiN in 780HE was 45.75 nm, while the average size of (Ti,Nb)C and (Ti,Nb,Mo)C was 17.23 nm and 3.59 nm, with corresponding densities of 88 /μm^2 and 45 /μm^2. When $t_{8/5}$ was 15 s~20 s, there was almost only TiN with the average size of 73.14 nm~85.57 nm in the microstructure. When $t_{8/5}$ was 30s, there was also some (Ti,Nb)C and (Ti,Nb,Mo)C in addition to TiN. The average size of TiN increased to 99.28 nm, and the average sizes of (Ti,Nb)C and (Ti,Nb,Mo)C with densities increased to 18.13 nm and 5.85 nm with the densities of 34 /μm^2 and 21 /μm^2.

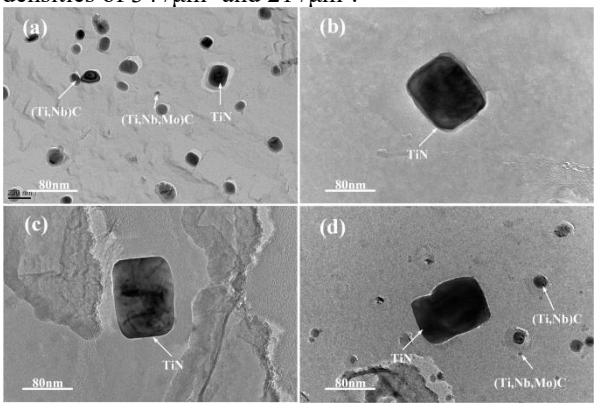

Fig. 5. Precipitates morphologies of 780HE and the coarse-grained zone amples with different cooling rates

3.4 Mechanical properties

3.4.1 Tensile property

The tensile properties of 780HE and the coarse-grained zone samples with different cooling rates were shown in Fig. 6. Obviously, the changing trend of ultimate strength and yield strength with cooling rate was consistent, but opposite for uniform elongation. Compared with 780HE, the strength and uniform elongation of the coarse-grained zone samples were reduced. As the cooling rate decreased, the yield strength and tensile strength first slightly decreased and then significantly increased, while the uniform elongation changed opposite. When $t_{8/5}$ was 20s, the yield strength were the lowest, at 708 MPa and 634 MPa, with the uniform elongation of 11 %. As the $t_{8/5}$ increased to 30s, the corresponding strength reached the maximum value with 789 MPa and 705 MPa. The uniform elongation was decreased to 10.4 %.

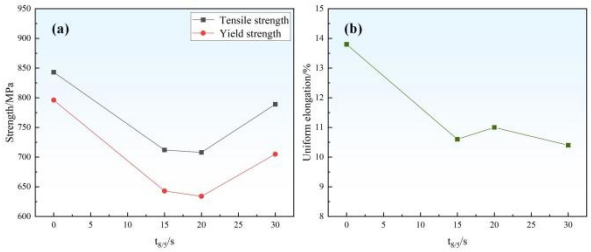

Fig. 6. Tensile properties of 780HE and coarse-grained zone samples with different cooling rates: (a)yield strength and ultimate strength; (b) total elongation.

3.4.2 Tensile property

Fig. 7 showed the impact properties of 780HE and the coarse-grained zone samples with different cooling rates. As the cooling rate decreases, the impact energy of the coarse-grained zone significantly decreased. When $t_{8/5}$ was 15s, the impact energy was 64.17 J, which was similar to 780HE. As $t_{8/5}$ increased to 20s and 30s , the impact energy decreased to 18.55 J and 5.73 J, respectively, which were approximately 29% and 10% of 780HE.

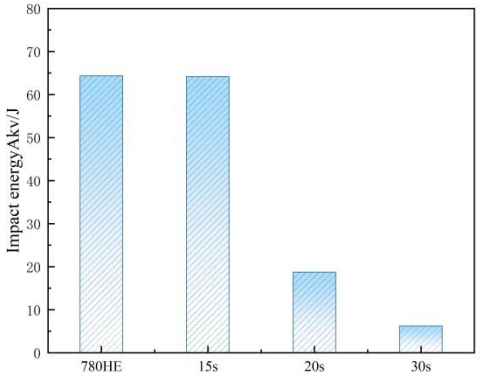

Fig. 7. Impact energy of 780HE and coarse-grained zone samples with different cooling rates

4 Discussions

4.1 The effects of cooling rate on the microstructures

The phase transition curves during cooling process of the coarse-grained zone samples with different cooling rates and the corresponding initial phase transition temperatures (Ar3) obtained using the tangent method were shown in Fig. 8. As the cooling rate decreased, the initial phase transition temperature decreased, but the variation was not significant. When $t_{8/5}$ was 15 s, the initial transition temperature of austenite was the lowest, at 553 ℃. As $t_{8/5}$ increased to 20 s and 30 s, the initial transformation temperature increased to 556 ℃ and 561 ℃, respectively. The decrease of the initial transition temperature increased the driving force for the nucleation and growth of lath bainite, but inhibited granular bainite, and increased the transformation rate of lath bainite. Therefore, with the increase of cooling rate, the content of lath bainite increased and the granular bainite decreased. However, due to the small difference in the initial transition temperature, there was little difference in the content of lath bainite with different cooling rates.

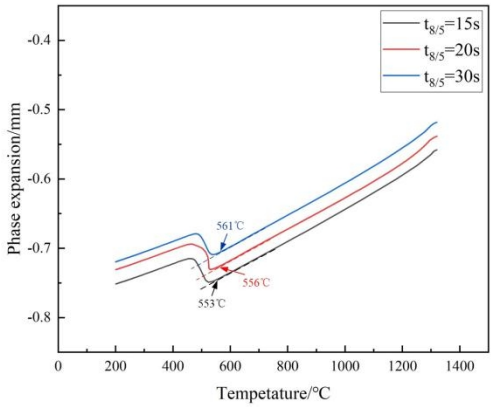

Fig. 8. Phase transition curves during cooling process of the coarse-grained zone samples with different cooling rates

4.2 The effects of cooling rate on the precipitates

The potential precipitates in the microstructure included TiN, TiC, NbN, NbC, MoC in theory. Researches showed that TiN had the highest TiN precipitated temperature. The mass fraction ratio of Ti to N in 780HE being 25, which was much higher than the ideal chemical ratio of 3.43 for TiN, there was no remaining (or very little) N bound to Nb.

According to the solubility product formulas (1)~(3), the initial precipitated temperatures of TiC, NbC, and MoC in austenite were calculated as 1797 ℃, 1095℃, and 1018 ℃. Considering the precipitation in austenite, the initial precipitation temperatures of TiC, NbC, and MoC in ferrite were calculated as 845 ℃,845 ℃, 673 ℃ by formulas (4)~(6). Obviously, TiN was not dissolved but grew during the thermal cycling with the peak temperature of 1320 ℃. Thus, with the decreased of cooling rates, the TiN size increased. During the heating process, TiC, NbC, and MoC dissolved, and there was no time to reprecipitate when $t_{8/5}$ shorter than 20 s. When $t_{8/5}$ was 30 s, the coarse-grained zone sample stayed longer below 1095 ℃ (Fig. 2), resulting in the reprecipitation of (Ti,Nb)C and (Ti,Nb,Mo)C.

The solubility product formulas of TiN [7] in austenite was

$$\log[(x_{Ti} \cdot x_N)]_\gamma = 3.94 - 15190/T, \quad (1)$$

where x_N (wt.%) were the solid solubility of Ti and N atoms, respectively; T (K) was the temperature. The solubility product formulas of TiC [8] in austenite was

$$\log[(x_{Ti} \cdot x_C)]_\gamma = 2.75 - 7000/T, \quad (2)$$

Where x_{Ti} (wt.%) and x_C (wt.%) was the solid solubility of Ti and C atoms. The solubility product formulas of NbC [7] in austenite was

$$\log[(x_{Nb} \cdot x_C)]_\gamma = 3.42 - 7900/T. \quad (3)$$

where x_{Nb} (wt.%) was the solid solubility of Nb atoms. The solubility product formulas of TiC, NbC and MoC in ferrite[9] were

$$\log[(x_{Ti} \cdot x_c)]_\alpha = 4.40 - 9575/T, \quad (4)$$
$$\log[(x_{Nb} \cdot x_c)]_\alpha = 3.90 - 9930/T, \quad (5)$$
$$\log[(x_{Mo} \cdot x_c)]_\alpha = 6.413 - 7982/T. \quad (6)$$

4.3 The effects of cooling rate on the strength

The strength of steel was a comprehensive result of solid solution strengthening, dislocation strengthening, precipitation strengthening, fine grain strengthening, and phase transformation strengthening. After undergoing different thermal cycles, the strengthening forms varied in different degrees except for solid solution strengthening. The methods for calculating the strength increments were cited the previous work[10].

The XRD patterns of 780FB and the coarse-grained zone samples with different cooling rates were shown in Fig. 9, and the corresponding dislocation densities were calculated by the W-H method[11] based on the FWHM. The calculated results were listed in Table 4, and the corresponding strength variations were plotted in Fig. 10. The dislocation densities in the coarse-grained region were higher than that in 780HE, and the strengthening effects were stronger. As the cooling rate decreased, the dislocation strengthening enhancement slightly decreased, with values of 36 MPa, 31 MPa, and 30 MPa, respectively. This was because the microstructures of coarse-grained zones were mainly composed of lath bainite, and the content had little difference under different cooling rates.

Table 4. The dislocation density of different samples

Samples	780HE	$t_{8/5}$=15s	$t_{8/5}$=20s	$t_{8/5}$=30s
Dislocation density (/mm^2)	1.50×10^7	2.55×10^6	2.32×10^6	2.27×10^6

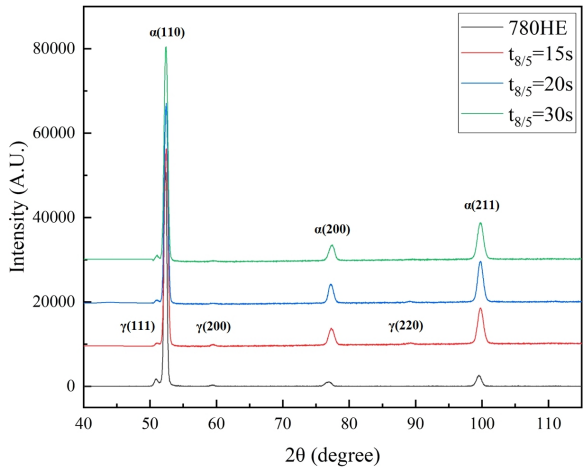

Fig. 9. XRD patterns of 780HE and coarse-grained zone samples with different cooling rates

According to chapter 3.3, the strength increments caused by precipitates were calculated as for coarse-grained zone samples with different cooling rates as -70MPa, -70MPa, and -28MPa, respectively, and the results were plotted in Fig. 10. Compared with 780HE, the precipitation strengthening in the coarse-grained zone was weakened, which was due to the reduction of precipitates. When $t_{8/5}$ was 15s~20s, the precipitation strengthening effect can be ignored for the few precipitates.

Based on the average effective grain size in Section 3.2, the strength increment variations caused by the fine grain strengthening for coarse-grained zone samples were -148 MPa, -150 MPa, and -153 MPa, respectively, as shown in Fig. 10. Results indicated that compared with 780HE, the grain sizes of coarse-grained zones had significantly increased, leading to a significant weakening of the fine grain strengthening effect.

The strengthening increments by phase transformation were calculated as 156 MPa, 141 MPa, and 137 MPa, respectively. Compared with 780HE, the strengthening effects of phase transformation in the coarse-grained zones were significant increased, since the content of lath bainite increased.

Results shew that compared with 780HE, the precipitation strengthening and fine grain strengthening effects weakened, while the dislocation strengthening and phase transformation strengthening effects enhanced. The main reason why the strength of 780HE was higher than that of the coarse-grained zone samples was that the fine grain strengthening effect significantly reduced in the coarse-grained zones. The stronger precipitation strengthening effect at $t_{8/5}$ of 30 s was significantly higher than that of 15 s and 20 s making the higher strength.

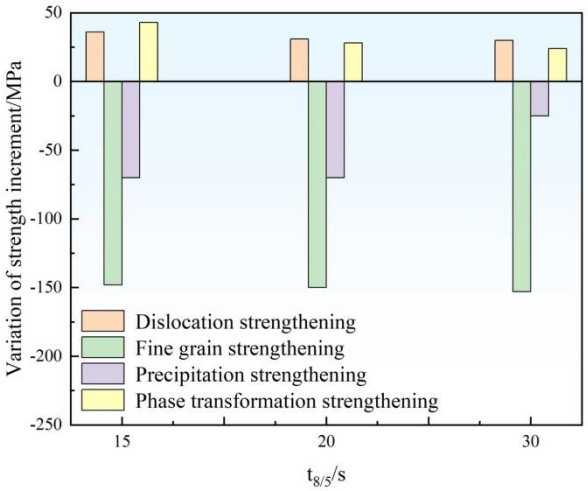

Fig. 10. The effects of cooling rate on the variations of strength increment

4.4 The effects of cooling rate on the impact properties

The factors that lead to differences in impact properties of the coarse-grained zones with different cooling rates may included microstructure, precipitates, grain size, and residual austenite.

Microstructure: The three coarse-grained zone samples were mainly composed of lath bainite accompanied by a small amount of granular bainite. The lath boundary approximately acted as the grain boundary, which hindered crack propagation. With the width of bainite lath decreased, the inhibitory effect on crack propagation enhanced.

Precipitates: The impact properties decreased with the size of precipitates increased, whether the precipitates were distributed at grain boundaries or independent in the matrix. From section 3.3, as the cooling rate decreased, the TiN size increased, thus the impact properties deteriorated.

Grain size: When the microcracks passed through grain boundaries from one grain to another, the slip direction of dislocations and the direction of crack propagation need to be changed due to changes in grain orientation. As the grain size became smaller, the changes in direction became more frequent, and consumed more energy. What's more, the larger number of grain boundaries, making the number of dislocations accumulated in front of the grain boundaries lower, which was beneficial for reducing stress concentration.

Residual austenite: Residual austenite can effectively improve the plastic deformation ability before crack initiation, thereby obtaining higher initiation energy, and improving the impact property. Based on Fig. 9, the content of residual Residual austenite were calculated as 2.2%, 1.6%, and 1.3%, repectively, which could be negligible.

According to section 3, with the cooling rate decreased, the size of grains and precipitates increased, and the width of lath bainite increased, leading to the decline of impact properties.

5 Conclusions

In this paper, the influential mechanism of cooling rate on the microhardness, microstructure, precipitates, and mechanical properties of the coarse-grained zone was systematically studied.The main conclusions were drawn as:

(1) The microstructure of coarse-grained zones were composed of bainite. As the cooling rate decreased, the lath bainite content decreased.

(2) When the cooling rate was 15s~20s, the precipitates were almost only TiN, the (Ti,Nb)C and (Ti,Nb,Mo)C reprecipitated as $t_{8/5}$ increased to 30s.

(3) As the cooling rate decreased, the yield strength and tensile strength first slightly decreased and then increased, while the uniform elongation changed opposite.

(4) As the cooling rates decreased, the impact properties significantly decreased.

References

1. M. Liu, J. Zhou, J. Zhang, C. Song, Q. Zhai, Mater. Charact., **190** (2022)
2. T. Senuma, M. Okayasu, H. Mohrbacher, Metals, **13** (2023)
3. C. Han, J. He, S. Yuan, J. Nets. Form. Eng., 2016
4. J. Liu, L. Hu, Y. Wang, Acta Metall. Sin., **3** (2004)
5. B. Njock, P. Kah, B. Mvola, P. Layus, X. Cai, Zavarivanje i Zavarene Konstrukcije, **65** (2024)
6. L. Yang, X. Wang, P. Huan, Z. Liu, M. Zhang, C. Chen, Z. Hu, Applied Laser, **38** (2018)
7. K. Narita, Trans. ISIJ Int., **15** (1975)
8. L. Yong, Z. Liu, X. Sun, J. Cao, X. Zha and Y. Zhang, Iron Steel Van. Titan., **26** (2005)
9. K. A. Tailor, Scr. Mater., 32(1995)
10. Y. Wang , X. Dong, Y. Yu, K. Hu, B. Yu, S. Chen, ISIJ Int., **68** (2024)
11. S. Takebayashi, T. Kunieda, N. Yoshinaga, K. Ushioda, S. Ogata: ISIJ Int., **50** (2010)